Multidimensional Engine Modeling: NO and Soot Emissions in a Diesel Engine with Exhaust Gas Recirculation

Hongsuk Kim*
Graduate School of Mechanical Engineering, Sunkyunkwan University, Kyunggi-do 440-746, *Korea*
Nakwon Sung
School of Mechanical Engineering, Sunkyunkwan University, Kyunggi-do 440-746, *Korea*

The effects of EGR(Exhaust Gas Recirculation) on heavy-duty diesel engine performance, NO and soot emissions were numerically investigated using the modified KIVA-3V code. For the fuel spray, the atomization model based on the linear stability analysis and spray wall impingement model were developed for the KIVA-3V code. The Zeldovich mechanism for the formation of nitric oxide and the soot model suggested by Hiroyasu et al. were used to predict the diesel emissions. In this paper, the computational results of fuel spray, cylinder pressure, and emissions were compared with experimental data, and the optimum EGR rates were sought from the NO and soot emissions trade-off. The results showed that the EGR is effective in suppressing NO but the soot emission was increased considerably by EGR. Using cooled EGR, soot emission could be enhanced without worsening of NO.

Key Words : Multidimensional Engine Modeling, Diesel Engine, Exhaust Gas Recirculation, NOx, Soot

Nomenclature

A, B: Constants
a, b : Reaction orders
C : Concentration
CN : Cetane number
E : Activation energy
K : Loss factor
L : Breakup length
M : Mass
N_a : Number of droplets after impingement
p : Pressure
R : Gas Constant
Re : Reynolds number
r : Droplet radius
r_f : Stochiometric oxygen mass
S_p : Mean piston speed
T : Temperature
t : Time
u_r : Relative velocity of a droplet
V_a : Intake air volume with EGR
V_o : Intake air volume without EGR
V_z : Injection velocity
We : Weber number

Greek Symbols

Λ : Wavelength of the fastest growing wave
β : Impinge angle
ε : Dissipation rate of turbulent kinetic energy
κ : Turbulent kinetic energy
μ : Viscosity
ρ : Density
σ : Surface tension
τ : Breakup time
τ_{id} : Ignition delay time
ω : Reaction rate

Subscripts

a : After impingement
b : Before impingement
f : Fuel

* Corresponding Author,
E-mail : hongsuk@nature.skku.ac.kr
TEL : +82-31-290-7498; **FAX** : +82-31-369-4503
Graduate School of Mechanical Engineering, Sunkyunkwan University, Kyunggi-do 440-746, Korea.
(Manuscript **Received** February 9, 2001; **Revised** May 8, 2001)

O_2 : Oxygen
s : Shed droplet after breakup or soot
sf : Soot formation
so : Soot oxidation
1 : Liquid jet
2 : Ambient gas

1. Introduction

Due to the growing concerns about the air pollution caused by diesel engines, NOx and particulate emission standards are becoming more stringent. Generally, the NOx emissions in a diesel engine could be reduced by the injection timing retardation, EGR (Exhaust Gas Recirculation), and aftertreatment technology. However, the application of injection timing retardation had a limitation due to its side effect on combustion. And to meet future emission standards, exhaust gas after treatment systems would be indispensable, but further study on current problems, such as deterioration of catalyst performance by particulate emission, would be needed. EGR was already being used on small size naturally aspirated diesel engines, and currently applied to turbocharged and intercooled heavy duty diesel engines with the modification of engine system to obtain adequate pressure difference for a self-sustained EGR flow rate. (Kohketsu et al., 1997)

The mechanism of NO reduction with EGR has been explored extensively. (Tsunemoto and Ishitani, 1980; Zelenka et al., 1998) Tsunemoto and Ishitani (1980) suggested that the effect of EGR on NO reduction might be due to two factors: lowering the combustion temperature with an increased heat capacity and a reduction of oxygen concentration in the cylinder charge. Zelenka et al. (1998) showed that the cooled EGR is indispensable to meet the NOx emission regulations in the future. According to their study on a venturi supported EGR system for a heavy -duty diesel engine, the cooled EGR reduced NOx emission level for EURO 3 standards without worsening fuel consumption.

Multidimensional engine modeling has been developed continuously as our basic understanding of the physics and chemistry of engine processes expands and as the capability of computers continues to increase. The aim of the present study is to show the multidimensional modeling capability of simulating the diesel engine processes and investigating the effects of EGR on diesel engine performance and emissions. Computation was performed by a KIVA-3V code. (Amsden, 1997) In order to get accurate results, the KIVA-3V code was modified in the spray, combustion and emission models.

2. Numerical Scheme

2.1 Spray model

The atomization of a liquid jet determines the size of droplet and influences greatly on combustion. The atomization model used in this study is based on the results of linear stability analysis by Liu et al. (1993) It is assumed that the injecting droplets at the nozzle exit have a characteristic size equal to the nozzle exit diameter. The radius of drops formed from a liquid jet is calculated using the stability analysis

$$r_s = B_o \Lambda \tag{1}$$

where $B_0=0.61$ is a constant, and Λ is the wavelength corresponding to the frequency of the fastest growing Kelvin-Helmholtz wave on the liquid surface. Λ is given by

$$\Lambda = \frac{9.02(1+0.45z^{0.5})(1+0.4T^{0.7})}{(1+0.865We_2^{1.67})^{0.6}} \tag{2}$$

where subscript 1 and 2 means a liquid jet and gas, respectively. The dimensionless variables are defined as: $Z=\sqrt{We_1}/Re_1$, $T=Z\sqrt{We_1}$, $We_2=\rho_2 u_r^2 r/\sigma$ $We_1=\rho_1 u_r^2 r/\sigma$, and $Re_1=u_r r\rho_1/\mu_1$. u_r is the magnitude of the relative velocity of a droplet. σ, ρ, and μ are surface tension, density, and viscosity, respectively. The parents droplet radius after breakup is calculated by the following expression:

$$\frac{dr}{dt} = \frac{r-r_s}{\tau} \tag{3}$$

where τ is the breakup time calculated as

$$\tau = \frac{L}{V_z} \tag{4}$$

where L is a breakup length and V_z is a injection velocity. Taylor(1962) considered the rate of mass loss per unit length of a jet and showed that the breakup length is given by

$$L/r=B_1\left(\frac{\rho_1}{\rho_2}\right)^{0.5}\frac{1}{f(T_a)} \tag{5}$$

$$T_a=\frac{\rho_1}{\rho_2}\left(\frac{Re_1}{We_1}\right)^2 \tag{6}$$

and the function $f(T_a)$ was approximated by Dan et al. (1997)

$$f(T_a)=\frac{\sqrt{3}}{6}[1-\exp(-10T_a)] \tag{7}$$

The constant B_1 has a value of 4.04 for typical diesel spray nozzles by Chehroudi et al. (1985)

To simulate the impingement of spray on a cylinder wall, the model suggested by Park and Watkins (1996) is used with the KIVA-3V code. The model was based on the experiment of a single water droplet impinging on a hot wall. When the Weber number of droplet before impingement is greater then 80, the droplet is breakup and rebounded. The number of droplets N_a after impingement are given by

$$N_a=0.00208\,We_b+7.8336 \tag{8}$$

Its tangential velocity after impingement does not change, but the normal velocity is reduced with a loss factor K. The loss factor K is calculated as following

$$K=\frac{1-We_a/We_b}{\cos^2\beta} \tag{9}$$

where We_a is the Weber number after impingement and β is the angle between the velocity vector of impinging drop and normal direction of wall. When We_b is less then 80, the droplet is rebounded without breakup and the change of velocity is calculated in a same manner of $We_b>80$.

2.2 Combution model

The ignition delay period is calculated by an empirical formula suggested by Hardenberg and Hase. (1981)

$$\tau_{id}(CA)=(1.43+0.22S_p)\times\exp\left[E_A\left(\frac{1}{RT}-\frac{1}{17{,}190}\right)\left(\frac{21.1}{p-12.4}\right)^{0.63}\right] \tag{10}$$

Table 1 Coefficients of Arrhenius combustion model

K_1(mol/cm^3·sec)	a	b	E(kJ/mol)
3.0×10^{10}	0.25	1.5	77.3

where S_p is the mean piston speed (m/s) and R is the universal gas constant (8.3143 J/mol K). Activation energy E_A is given by

$$E_A=\frac{618840}{CN+25} \tag{11}$$

where CN is a fuel cetane number. T and p are temperature (K) and pressure(bar) at TDC.

To describe the diesel engine combustion, one step global reaction mechanism is considered. Tetradecane ($C_{14}H_{30}$) is used as the fuel due to its similar C/H ratio to the commonly used diesel fuel.

$$C_{14}H_{30}+21.5(O_2+3.72N_2)\rightarrow 14CO_2+15H_2O+79.98N_2 \tag{12}$$

It is postulated that combustion is controlled by chemical kinetics at the initial combustion stage and later by turbulent diffusion combustion. The reaction rate of combustion controlled by chemical kinetics can be expressed as

$$\omega_1=K_1EXP\left(\frac{-E}{RT}\right)\cdot(C_f)^a(C_{O2})^b \tag{13}$$

where C is the concentration of species. Subscripts f and O_2 mean fuel and oxygen, respectively. Pre-exponential factor K_1, reaction orders a and b, and activation energy E used in this study are listed at Table 1.

Reaction rate of the turbulent diffusion combustion can be expressed as

$$\omega_2=B\frac{\varepsilon}{k}\min\left(C_f,\frac{C_{O2}}{r_f}\right) \tag{14}$$

where r_f is the stochiometric oxygen requirement to burn 1 kg fuel, ε is the rate of dissipation of turbulent kinetic energy, and k is the turbulent kinetic energy. A model constant $B=40$ is used in this study.

2.3 Emission models

In the soot emission model suggested by Hiroyasu et al. (1989), the rate of change of soot

mass is calculated from the rate of soot formation and oxidation,

$$\frac{dM}{dt}=\dot{M}_{sf}-\dot{M}_{so} \tag{15}$$

where M_s, $\dot{M}_{sf}$ and $\dot{M}_{so}$ mean soot mass, soot formation rate, and oxidation rate, respectively. The soot formation rate is given by

$$\dot{M}_{sf}=A_f M_{fv} P^{0.5}\exp\left(-\frac{E_f}{RT}\right) \tag{16}$$

where M_{fv} is the fuel vapor mass. A model constant A_f is 150, and activation energy of formation E_f is 12500 cal/mol. The soot oxidation rate is given by

$$\dot{M}_{so}=A_o M_s \frac{P_{O_2}}{P} P^{1.8}\exp\left(-\frac{E_o}{RT}\right) \tag{17}$$

where M_s is the soot mass. A model constant A_o is 300, and activation energy of oxidation E_o is 14000 cal/mol.

The NO emission is evaluated by the Zeldovich mechanism.

$$O_2+2N_2 \leftrightarrow 2NO+2N \tag{18}$$
$$N_2+2O_2 \leftrightarrow 2NO+2O \tag{19}$$
$$N_2+2OH \leftrightarrow 2NO+2H \tag{20}$$

The mechanism of prompt NO formed in some combustion environments such as in the low-temperature, fuel-rich zones is neglected in this study.

3. Condition for Calculation

The specifications of a diesel engine are given in Table 2. The computational meshes are shown in Fig. 1. The total number of cells is about 35000 at IVC, which is the available maximum number for running by a 500MHz Pentium PC under consideration of computational efficiency. Full mesh is used due to the offset of bowl. The calculation starts from IVC and ends at EVO. As an initial condition, the gas temperature, pressure, and species densities were assumed to be uniform throughout the entire combustion chamber. The initial velocity distribution is assumed to be a swirl profile in a cylinder. The calculation conditions of full and part load are presented in Table 3. The injection flow rates given by Kim (1995) are used. The EGR rate is defined as

Table 2 Engine specifications

Displacement (l)	11.051
Bore* Stroke(mm)	123.0*155.0
Connecting rod(mm)	275.0
Compression ratio	17.1
Valve timing	IVO 18° CA ATDC
	IVC 34° CA ABDC
	EVO 46° CA ABDC
	EVC 14° CA BTDC
Injector hole number	5
Nozzle diameter (cm)	0.029

Table 3 Calculation conditions

RPM	1400
Power (ps)	112.5, 85.0
Fuel amount (g/st)	0.1013, 0.077
Injection timing (baseline)	6° BTDC~10°ATDC
Air/Fuel ratio	19.0, 25.0
Swirl ratio	2.5
Cylinder wall temp. (K)	405
Cylinder head temp. (K)	486
Piston surface temp. (K)	578
Air temp at IVC (K)	344
Cylinder pressure at IVC (bar)	1.04

$$EGR_{rate}=\frac{Vo-Va}{Vo}\times 100 \tag{21}$$

where Vo is intake air volume without EGR and is intake air volume with EGR. Species mass fractions of the air without EGR at IVC are N_2 76.5%, O_2 22%, CO_2 1%, and H_2O 0.5%. When EGR is applied, the initial species mass fractions are determined using the exhaust gas composition calculated without EGR.

4. Results and Discussion

4.1 Model validation

The results from the spray models are compared with the spray experiments by Alloca and Fusco. (1994) Their measurements were performed under 1.7 MPa nitrogen at room tem-

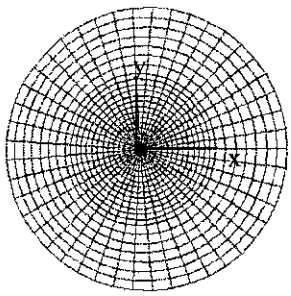

(a) View at the cross-section of z=18.3cm

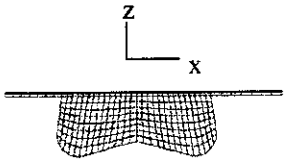

(b) View at the cross-section of y=0cm

Fig. 1 Computational grids of the combustion chamber at TDC

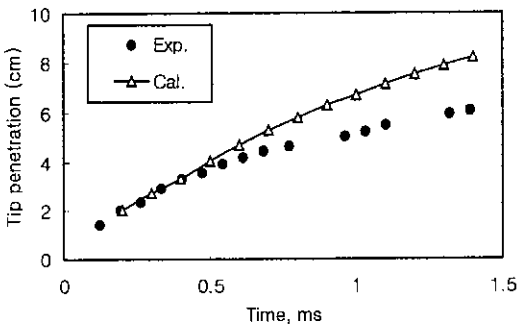

Fig. 2 Comparison of calculated spray tippenetration with measurements by Alloca et al. (1994)

perature using a n-heptane fuel. The nozzle diameter of the injector is 0.2 mm, and the maximum injection pressure is about 60 MPa with delivered fuel flowrate of 14.4 mm^3/st. Figure 2 shows the comparison between calculated results of spray tip-penetration and experimental data. The calculated tip-penetration overestimates the experimental data, and linearly increased with respect to time. Figure 3 presents the comparison of measured and computed SMR at 20 mm downstream of spray. The calculated SMR agree well with the measurements. Figure 4 shows the comparison of measured and computed SMR along the spray axis at 1.3 ms from the start

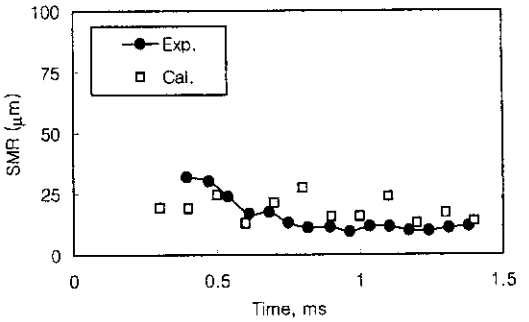

Fig. 3 Comparison of calculated SMR with experimental results measured by Alloca et al. (1994) at 20mm downstream the spray axis

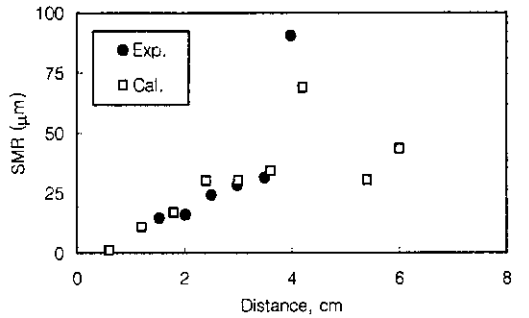

Fig. 4 Comparison of calculated SMR with experimental results measured by Alloca et al. (1994) with respect to the distance from the nozzle at 1. 3ms after start of injection

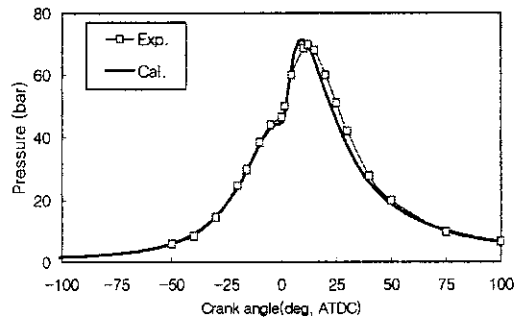

Fig. 5 Comparison of measured and calculated pressures at a full load, measured data by Kim(1996)

of injection. The experimental drop size increases along the axis due to coalescence effects. The calculation results agree well with the experiments.

The calculated and measured cylinder pressures

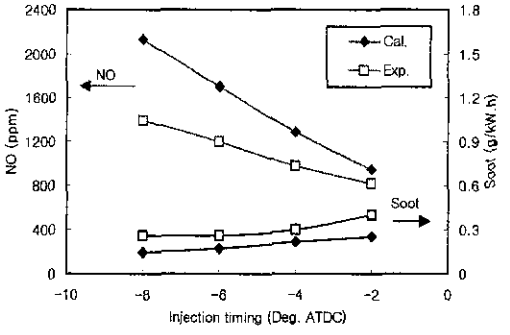

Fig. 6 Comparison of measured and calculated emissions with respect to injection timing at full load measured data by Kim(1996)

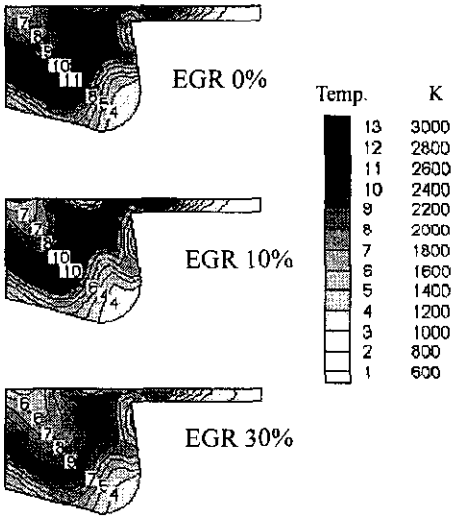

Fig. 7 Effect of EGR rates on the local temperature in a cylinder (10 ATDC , full load)

are compared in Fig. 5. Measured data are from the experiments by Kim. (1996) The pressures are overestimated at the initial stage of combustion and underestimated as the combustion process proceeds. The emission results with respect to the injection timing are shown in Fig. 6. NO is reduced but soot is increased with injection timing retardation. It is found that the emission trend of calculation is similar to that of measurements.

4.2 Combustion and emission characteristics with EGR

The EGR is well known to reduce NOx by lowering combustion temperature. Figure 7 shows

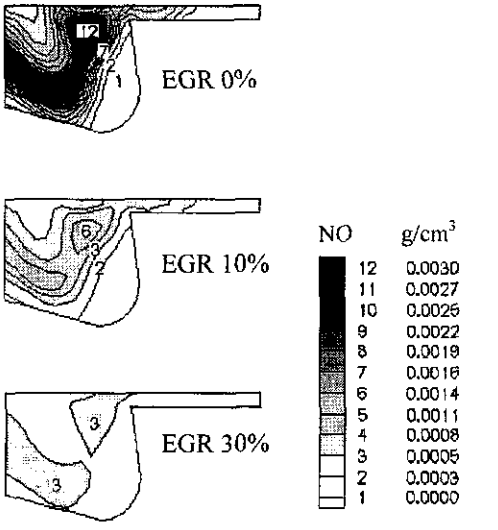

Fig. 8 Effect of EGR rates on the NO formation in a cylinder (10 ATDC, full load)

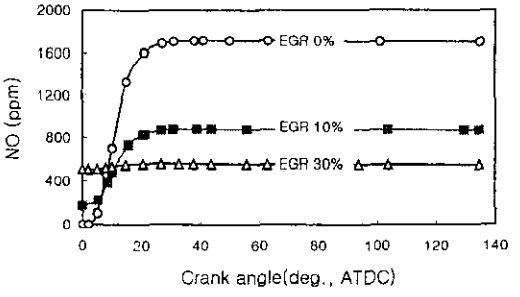

Fig. 9 NO formation with EGR rates at a full load

the effect of EGR on local temperature in a combustion chamber at 10 ATDC at a full load. The level of local temperature is decreased with the increased EGR rate due to the increased heat capacity of the EGR gas and the incomplete combustion. Figure 8 shows the effect of EGR on NO formation in a cylinder. NO is formed actively in the region of high temperature and the level of NO is reduced with the increased EGR rate. NO formation with respect to crank angle is presented in Fig. 9. The NO is mainly generated in the initial part of combustion before 20° ATDC. As the EGR rate is increased, the NO formation is drastically decreased at the early stage of combustion process. With the 30% EGR rate, it is found that NO is not formed in the combustion process and about 500ppm of NO is

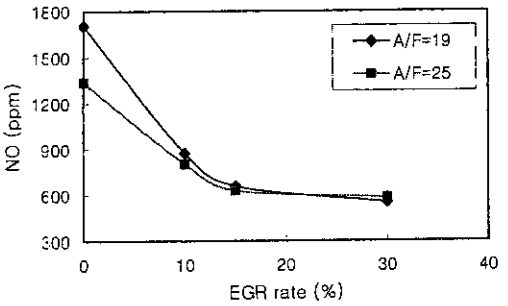

Fig. 10 Effect of EGR rates on NO emission at EVO

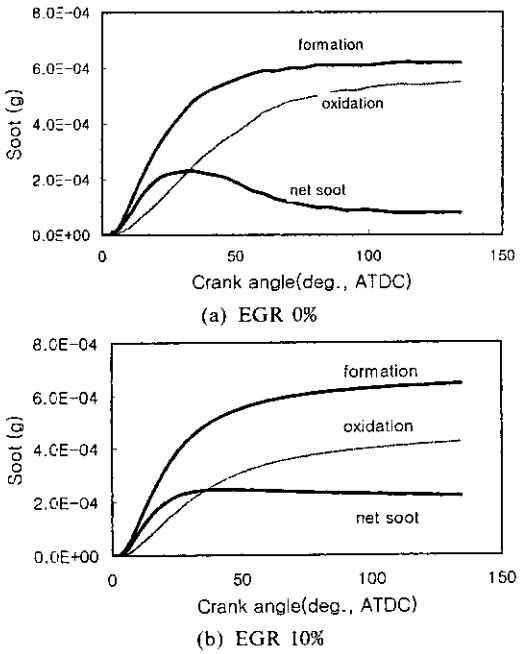

Fig. 11 Soot formation and oxidation with EGR rates at full load

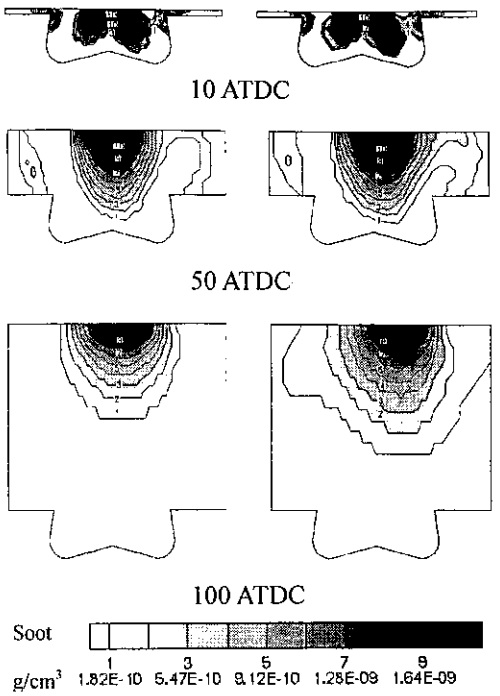

Fig. 12 Effect of EGR rates on soot density at full load

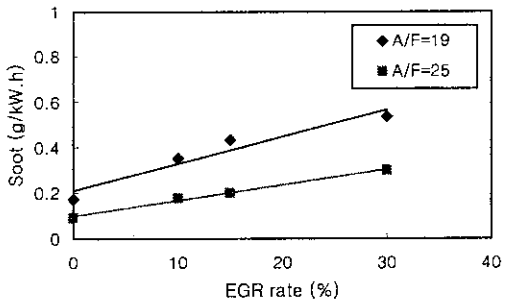

Fig. 13 Effect of EGR rates on soot emissions at EVO

from the recirculated exhaust gases. Figure 10 shows the NO emission at EVO. When EGR rate is exceeded 10%, NO emission is not remarkably reduced any more at both full and part load.

Soot formation and oxidation characteristics with EGR rates are presented in Fig. 11. As the combustion process proceeds, the soot formation and oxidation occur simultaneously. The soot formation is dominant at the early part of the combustion process, while oxidation is dominant at the latter part of the combustion process. From the comparison of Fig. 11 (a) and Fig. 11 (b), it is found that the soot oxidation rate of EGR 10% is less than that of EGR 0% due to the deficiency of O_2. The increase of net soot emission with EGR is due to the deterioration of the soot oxidation.

Figure 12 shows soot distribution in a cylinder. The soot exists in the center of combustion chamber following the spray at 10° ATDC. At 50° ATDC, the soot forming area is increased a little by the expansion process. At 100° ATDC, the reduction of soot level can be seen due to oxidation. Figure 13 shows the soot amounts with EGR rates at EVO. The soot emission is increased linearly with EGR rates. The soot formation at

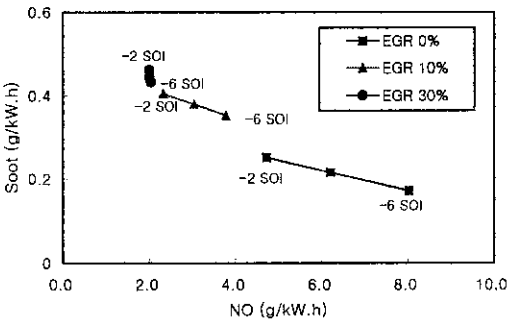

Fig. 14 Effect of EGR rates on the soot and NO emissions at full load with different injection timing

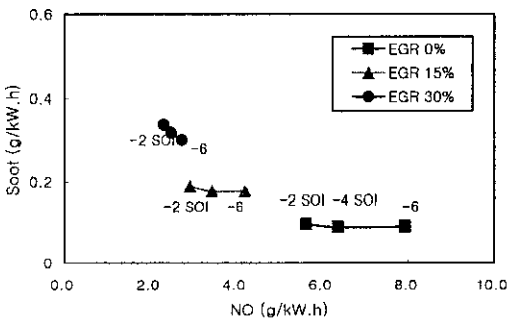

Fig. 15 Effect of EGR rates on the soot and NO emissions at part load with different injection timing

part load is less than that of full load because of the sufficient air.

The determination of optimum EGR rate is necessary because soot is increased with EGR. The trade-off in emissions is shown in Figs. 14 and 15. The effect of injection timing on the emission characteristics is also presented. It is found that the optimum EGR rates are 10% at full load and 15% at part load. The EGR deteriorates combustion because of the reduction in O_2. The reduction of IMEP with respect to EGR rates is presented in Fig. 16. With an increase in the EGR rates, the IMEP is linearly decreased. About 12% reduction of IMEP occurs at the optimum EGR rates at the full and part load conditions.

To investigate the cooled EGR characteristics, the EGR gas is cooled from 613K to 413K at the optimum EGR rate of full load. Figure 17 shows the effect of the cooled EGR on the bulk temperature in a cylinder. The bulk temperature is de

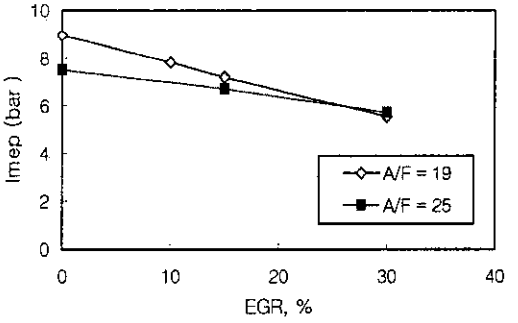

Fig. 16 Effect of EGR rates on IMEP

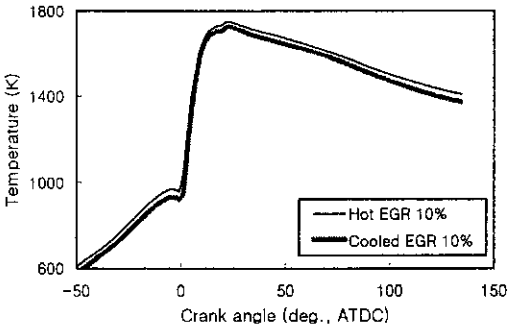

Fig. 17 The effect of the hot and cooled EGR on bulk temperature at full load

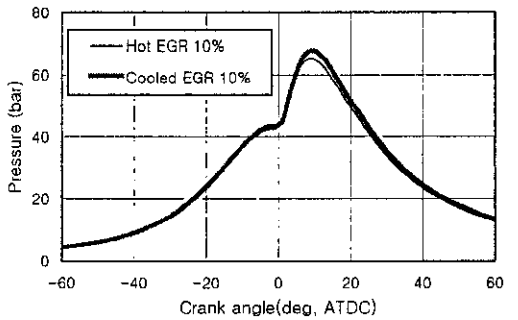

Fig. 18 The effect of the hot and cooled EGR on cylinder pressure at full load

creased with the cooled EGR in the combustion process, because cooled EGR increases the heat capacity. Figure 18 shows the effect of cooled EGR on cylinder pressures. The cylinder pressure of the cooled EGR is higher than that of the hot EGR due to enhanced combustion. The effect of cooled EGR on emissions is shown in Fig. 19. The 22% soot and 7% NO emissions are reduced by cooling the EGR compared with emissions of hot EGR. From this results, it is found that the

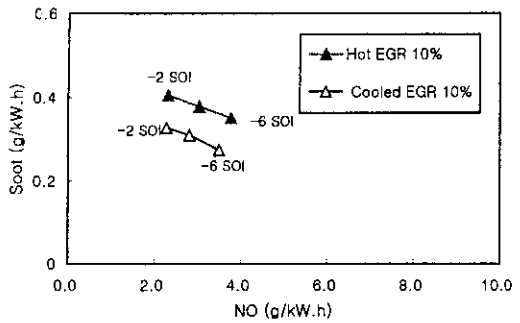

Fig. 19 The effect of the cooled EGR on the soot and NO at full load

effectiveness of EGR in suppressing NO and soot emissions was enhanced considerably by the cooled EGR.

5. Conclusions

To conduct the multidimensional engine modeling of a heavy-duty diesel engine, the modified version of a KIVA-3V code was used. The details of the spray, combustion and emission models were presented in this paper. The calculated results are in good agreements with experiments. The effects of EGR on the diesel engine performance and emissions could be summarized as follows:

(1) The optimum EGR rates were 10% at the full load and 15% at the part load of 1400rpm.

(2) About 12% IMEP was reduced with the optimum EGR rates for the full and part loads at 1400 rpm.

(3) NO was reduced effectively by EGR, but soot emissions was increased considerably. Using cooled EGR, soot emission could be enhanced without worsening of NO.

Reference

Alloca L., Corcione F. E., and Fusco A., 1995 "Modeling of Diesel Spray Dynamics and Comparison with Experiments," SAE paper No. 941895.

Amsden A. A., 1997, "KIVA-3V: A Block-Structured KIVA Program for Engines with Vertical or Canted Valves," Los Alamos National Laboratory report LA- 13313-MS (July)

Chehroudi B. and Bracco F. V., 1985, "On the Intact Core of Full cone Sprays," Soc. Sutomot. Eng. Tech. Paper No. 850126.

Dan T., Takagishi S., Senda J., and Fujimoto H., 1997, Effect of Ambient Gas Properties for Characteristics of Non-Reacting Diesel Fuel Spray , SAE Paper No. 970352.

Hardenberg H. O., and Hase F. W., 1981, "Ignition Improvers for ethanol Fuels," SAE paper No. 810249.

Hiroyasu H., and Nishida K., 1989, "Simplified Three-Dimensional Modeling of Mixture Formation and Combustion in a D. I. Diesel Engine," SAE paper No. 890269.

Kim S., 1996, "Study on the High Pressure Injection and the Reduction of Regulated Emissions in D. I. Diesel Engine," Ph. D. thesis, Seoul National Univ.

Kohketsu S., Mori K., Sakai K., and Hakozaki T., 1997, "EGR Technologies for a Turbocharged and Intercooled Heavy-Duty Diesel Engine," SAE paper No. 970340.

Liu A. B., Mather D., and Reitz R. D., 1993, "Modeling the Effects of Drop Drag and Breakup on Fuel Sprays," SAE Paper No. 930072.

Park K., and Watkins A. P., 1996, "Assessment and Application of a New Spray Wall Impaction Model," IMechE C499/044/96.

Taylor G. I., 1962, "Generation of Ripples by Wind Blowing over Viscous Fluids," pp. 244 ~254, Cambridge Univ. press.

Tsunemoto H. and Ishitani H., 1980, "The Role of Oxygen in Intake and Exhaust on NO Emission, Smoke and BMEP of a Diesel Engine with EGR system," SAE paper No. 800030.

Zelenka P., Aufinger H., Reczek W. and Cartellier W., 1998, "Cooled EGR-A Key Technology for Future Efficient HD Diesels," SAE paper No. 980190.